21st International Symposium on
Mathematical Theory of Networks and Systems
July 7-11, 2014. Groningen, The Netherlands

Basis Selection and Closure for POD Models of Convection Dominated Boussinesq Flows*

Omer San[1] and Jeff Borggaard[2]

Abstract— **We present two challenging benchmark problems for creating reduced-order models for the unsteady Boussinesq equations. The first is a differentially-heated cavity flow in the quasi-periodic regime and the second is an unsteady Marsigli flow problem exhibiting the Kelvin-Helmholtz instability. The first can be modeled accurately using the principle interval decomposition (PID), which optimizes the length of time windows over which to perform the POD procedure and is highly effective in convective problems. The second benchmark problem requires the introduction of stabilization terms that capture the effect of energy dissipation that is missing in a truncated POD basis. We provide two eddy viscosity stabilization models and optimize the parameter selection to best represent simulation data. These benchmark problems demonstrate the feasibility of low-order nonlinear models for capturing the dynamics of complex thermal fluid behavior and can be used to validate alternative reduced-order modeling methodologies.**

I. INTRODUCTION

Proper orthogonal decomposition (POD) is one of the most successful reduced-order modeling techniques for nonlinear systems. POD has been used to generate a representative reduced-order model (ROM) for the control, optimization and analysis for a large number problems in fluid systems (see for example, [1]–[4]). POD extracts the most energetic modes from a collection of high fidelity numerical simulations of the governing equations and are generally parameter dependent. These bases are then used to reduce the governing equations into a truncated system of amplitude equations using the Galerkin projection. The resulting systems are low-dimensional and provide an efficient framework for post-processing analysis, optimization and control applications.

For many flows, the POD-Galerkin method provides an efficient and accurate way to generate reduced-order models. However, its applicability to complex convective flows is limited due to the errors associated with the finite truncation in POD modes. Several successful stabilization methods have been suggested in order to model the effects of discarded POD modes [5]–[8]. In many of these approaches, conjectures used to stabilize POD models resemble closure models of large eddy simulations for turbulent flows [9], [10].

Although most reduced-order modeling studies have been performed by considering flows without thermal effects, the POD approach has also been applied to a number of thermal-fluids problems governed by incompressible Boussinesq equations. It has been used by Sirovich and Deane [11], [12] for Rayleigh-Bénard convection problems. Gunes and co-workers [13], [14] applied POD to two-dimensional convective flows differentially-heated from the sides. Sahan et al. [15] used a POD model in order to investigate translational flows and heat transfer characteristics in a periodically grooved channel. Podvin and Le Quere [16] utilized POD to obtain a reduced-order model to study the two-dimensional buoyancy-driven flow in a differentially-heated tall cavity. POD based reduced-order models of thermally driven two-dimensional flows in a horizontal rotating cylinder, subject to the Boussinesq approximation, have been studied by Hasan and Sanghi [17]. A common objective in all of these studies is to determine how well low-dimensional models can reproduce the flow dynamics.

In the present study, we construct a reduced-order model based on POD for the two-dimensional Boussinesq equations using the vorticity-stream function formulation. This results in a coupled set of ordinary differential amplitude equations for the vorticity and temperature fields. The current work aims to demonstrate the applicability and limitations of POD-ROM for Boussinesq systems with applications to both quasi-periodic and complex convective flows. To minimize the numerical discretization error, a fourth-order compact finite difference scheme is used to obtain accurate snapshots as well as to compute any spatial derivatives required by the model. The use of high-order numerical schemes to construct the high-fidelity data for the reduced-order model also helps to decouple the numerical effects from the POD modeling effects, and serves as a guide in the subsequent interpretation of the POD reduced-order modeling results. A simplified eddy viscosity-type stabilization method is also presented and tested for a lock-exchange problem. The strong shear flow induced by a temperature jump results in the Kelvin-Helmholtz instability, which can be considered quite a challenging test problem for the assessment of reduced-order models in convective Boussinesq flows.

The organization of this paper is as follows. The incompressible Boussinesq equations are presented in Section II. The derivation of POD-ROM is presented in Section III. The numerical schemes for the mathematical models utilized in this paper are briefly described in Section IV. In Section V, the POD-ROM is tested for the differentially-heated cavity flow problem and then for a more challenging the convective flow setting known as Marsigli or lock-exchange problem at $Re = 5000$. Finally, Section VI contains concluding remarks.

*This work was supported by the National Science Foundation under contract DMS-1016450.

[1]Omer San is with the Interdisciplinary Center for Applied Mathematics, Virginia Tech, Blacksburg, VA 24061, USA omersan@vt.edu

[2]Jeff Borggaard is with the Department of Mathematics and the Interdisciplinary Center for Applied Mathematics, Virginia Tech, Blacksburg, VA 24061, USA jborggaard@vt.edu

ISBN: 978-90-367-6321-9

II. GOVERNING EQUATIONS

The dimensionless form of the two-dimensional incompressible Boussinesq equations on a domain Ω is given by

$$\nabla \cdot \mathbf{u} = 0, \tag{1}$$

$$\frac{\partial \mathbf{u}}{\partial t} + \mathbf{u} \cdot \nabla \mathbf{u} = -\nabla p + \frac{1}{Re}\Delta \mathbf{u} + Ri\ \theta\ \hat{\mathbf{j}}, \tag{2}$$

$$\frac{\partial \theta}{\partial t} + \mathbf{u} \cdot \nabla \theta = \frac{1}{RePr}\Delta \theta \tag{3}$$

where $\boldsymbol{u} = (u, v)^T$ is the velocity with horizontal and vertical components represented by u and v, respectively, p is the pressure, and θ is the temperature. The Boussinesq equations are generally characterized by three dimensionless numbers. Re is the Reynolds number, the ratio of viscous effects to the inertial effects; Pr is the Prandtl number, the ratio of the kinematic viscosity to the heat conductivity; and Ri is the Richardson number, the ratio of the buoyancy force to the inertial forces.

Instead of the primitive variable formulation given by (1)-(3), we introduce the vorticity $\omega = (\nabla \times \boldsymbol{u}) \cdot \widehat{\mathbf{k}}$ and the stream function ψ. The governing equations for two-dimensional incompressible Boussinesq equations can be written as the two coupled scalar transport equations

$$\frac{\partial \omega}{\partial t} + \frac{\partial \psi}{\partial y}\frac{\partial \omega}{\partial x} - \frac{\partial \psi}{\partial x}\frac{\partial \omega}{\partial y} = \frac{1}{Re}\Delta \omega + Ri\frac{\partial \theta}{\partial x}, \tag{4}$$

$$\frac{\partial \theta}{\partial t} + \frac{\partial \psi}{\partial y}\frac{\partial \theta}{\partial x} - \frac{\partial \psi}{\partial x}\frac{\partial \theta}{\partial y} = \frac{1}{RePr}\Delta \theta, \tag{5}$$

along with the kinematic relationship between vorticity and stream function given by

$$\frac{\partial^2 \psi}{\partial x^2} + \frac{\partial^2 \psi}{\partial y^2} = -\omega. \tag{6}$$

The desired flow velocity components are

$$u = \frac{\partial \psi}{\partial y}, \quad v = -\frac{\partial \psi}{\partial x}. \tag{7}$$

III. REDUCED-ORDER MODELING

In this section, we present the POD for model reduction of the unsteady, incompressible Boussinesq equations given by (4)-(5). We construct our POD-ROM by computing basis functions from the field variables ω and θ then applying Galerkin projection using a high-order compact difference scheme described in Section IV.

A. Computing POD Basis Functions

In the time stepping process of solving (4)-(5), the ith record of any field variable ζ (i.e., the vorticity field ω or temperature field θ in this study) at time $t = t_i$ is denoted $\zeta^i(x, y)$ for $i = 1, 2, ..., M$ where M is a large enough number of snapshots to identify representative flow information. We construct the temporal autocorrelation matrix from these linearly independent records as

$$C_{ij} = \int_\Omega \zeta^i(x, y)\zeta^j(x, y)dxdy, \tag{8}$$

where Ω is the entire spatial domain in which the field variables are defined, and i and j refer to the ith and jth snapshots. Note that the autocorrelation matrix C is a non-negative Hermitian matrix. Finding eigenvalues for C can be used to calculate right singular vectors for $\zeta^i(x, y)$ from which we can compute the POD basis functions (e.g., see [18]–[20]). If we write the eigenvalue problem as

$$C\Upsilon = \Upsilon\Lambda, \tag{9}$$

where $\Lambda = \text{diag}[\lambda_1, \lambda_2, ..., \lambda_M]$ has eigenvalues listed in descending order and and $\Upsilon = [\boldsymbol{\upsilon}^1, \boldsymbol{\upsilon}^2, ..., \boldsymbol{\upsilon}^M]$ contains the corresponding eigenvectors, the kth POD basis function associated with the field variable ζ, ϕ_k can be computed as

$$\phi_k(x, y) = \frac{1}{\lambda_k}\sum_{i=1}^{M} \upsilon_i^k \zeta^i(x, y), \tag{10}$$

where υ_i^k is the ith component of eigenvector $\boldsymbol{\upsilon}^k$. The eigenvectors are normalized to ensure the orthogonality condition

$$(\phi_k, \phi_l) = \begin{cases} 1, & k = l; \\ 0, & k \neq l. \end{cases} \tag{11}$$

Using the kinematic relationship between stream function and vorticity given by Eq. (6), the jth basis function for the stream function, $\phi_j^\psi(x, y)$, can be obtained from the jth vorticity basis function by solving a Poisson equation

$$\frac{\partial^2 \phi_j^\psi}{\partial x^2} + \frac{\partial^2 \phi_j^\psi}{\partial y^2} = -\phi_j^\omega. \tag{12}$$

B. Galerkin Projection to Obtain ROM

To obtain a reduced-order model, we compute R POD basis functions for the fluctuations of field variables ω and θ from their (temporal) mean values, $\bar{\omega}$ and $\bar{\theta}$ (where $1 \leq R \leq M$). Then represent the scalar field variables as

$$\omega(x, y, t) = \bar{\omega}(x, y) + \sum_{k=1}^{R} \alpha_k(t)\phi_k^\omega(x, y), \tag{13}$$

$$\theta(x, y, t) = \bar{\theta}(x, y) + \sum_{k=1}^{R} \beta_k(t)\phi_k^\theta(x, y), \tag{14}$$

where we now need to determine dynamical equations for the time dependent coefficients $\{\alpha_k\}$ and $\{\beta_k\}$. To obtain these dynamical systems for the coefficients, we rearrange (4)-(5) using linear and nonlinear operators in the following

$$\frac{\partial \omega}{\partial t} = N[\omega; \psi] + \frac{1}{Re}L[\omega] + RiD[\theta], \tag{15}$$

$$\frac{\partial \theta}{\partial t} = N[\theta; \psi] + \frac{1}{RePr}L[\theta], \tag{16}$$

where L and D are linear operators, and N is the nonlinear operator given by

$$L[f] = \Delta f, \quad D[f] = \frac{\partial f}{\partial x}, \quad N[f; g] = \nabla f \times \nabla g, \tag{17}$$

where f and g are arbitrary field variables.

Next, we apply Galerkin projection to the system by multiplying (15)-(16) with the basis functions and integrate

over the domain. The Galerkin projection onto the kth basis function can be written as

$$\Big(\frac{\partial\omega}{\partial t},\phi_k^\omega\Big)=\Big(N[\omega;\psi],\phi_k^\omega\Big)+\frac{1}{Re}\Big(L[\omega],\phi_k^\omega\Big)+Ri\Big(D[\theta],\phi_k^\omega\Big), \tag{18}$$

$$\Big(\frac{\partial\theta}{\partial t},\phi_k^\theta\Big)=\Big(N[\theta;\psi],\phi_k^\theta\Big)+\frac{1}{RePr}\Big(L[\theta],\phi_k^\theta\Big). \tag{19}$$

Substituting (13)-(14) into (18)-(19), and using the orthogonality condition given by (11), we obtain the following coupled POD reduced-order system for $k=1,2,\ldots,R$:

$$\frac{d\alpha_k}{dt}=B_k^\omega+\sum_{i=1}^{R}P_{ik}^\omega\alpha_i+\sum_{i=1}^{R}H_{ik}^\omega\beta_i+\sum_{i=1}^{R}\sum_{j=1}^{R}Q_{ijk}^\omega\alpha_i\alpha_j, \tag{20}$$

$$\frac{d\beta_k}{dt}=B_k^\theta+\sum_{i=1}^{R}P_{ik}^\theta\beta_i+\sum_{i=1}^{R}H_{ik}^\theta\alpha_i+\sum_{i=1}^{R}\sum_{j=1}^{R}Q_{ijk}^\theta\beta_i\alpha_j, \tag{21}$$

where

$$B_k^\omega=\frac{1}{Re}\big(L[\bar\omega],\phi_k^\omega\big)+\big(N[\bar\omega;\bar\psi],\phi_k^\omega\big)+Ri\big(D[\bar\theta],\phi_k^\omega\big), \tag{22}$$

$$B_k^\theta=\frac{1}{RePr}\big(L[\bar\theta],\phi_k^\theta\big)+\big(N[\bar\theta;\bar\psi],\phi_k^\theta\big), \tag{23}$$

$$P_{ik}^\omega=\frac{1}{Re}\big(L[\phi_i^\omega],\phi_k^\omega\big)+\big(N[\bar\omega;\phi_i^\psi]+N[\phi_i^\omega;\bar\psi],\phi_k^\omega\big), \tag{24}$$

$$P_{ik}^\theta=\frac{1}{RePr}\big(L[\phi_i^\theta],\phi_k^\theta\big)+\big(N[\phi_i^\theta;\bar\psi],\phi_k^\theta\big), \tag{25}$$

$$H_{ik}^\omega=Ri\big(D[\phi_i^\theta],\phi_k^\omega\big), \tag{26}$$

$$H_{ik}^\theta=\big(N[\bar\theta;\phi_i^\psi],\phi_k^\theta\big), \tag{27}$$

$$Q_{ijk}^\omega=\big(N[\phi_i^\omega;\phi_j^\psi],\phi_k^\omega\big), \tag{28}$$

$$Q_{ijk}^\theta=\big(N[\phi_i^\theta;\phi_j^\psi],\phi_k^\theta\big). \tag{29}$$

The proper orthogonal decomposition reduced-order model (POD-ROM) given by (20)-(21) consists of $2R$ coupled ordinary differential equations and can be solved easily by a standard numerical method (e.g., we use a third-order Runge-Kutta scheme in this study). We should emphasize that the degrees of freedom of the system have been substantially decreased and the resulting dynamical system can be solved very efficiently since all the POD basis functions and corresponding model coefficients in (22)-(29) are precomputed from the simulation snapshots.

In this study, we focus on the predictive capabilities of various POD reduced-order models for the complex flow problems in Boussinesq system. To complete the dynamical system given by (20)-(21), the initial conditions are specified by using the following projection

$$\alpha_k(t_0)=\Big(\omega(x,y,t_0)-\bar\omega(x,y),\phi_k^\omega\Big), \tag{30}$$

$$\beta_k(t_0)=\Big(\theta(x,y,t_0)-\bar\theta(x,y),\phi_k^\theta\Big), \tag{31}$$

where $\omega(x,y,t_0)$ and $\theta(x,y,t_0)$ are the initial conditions for the vorticity and temperature fields, respectively, specified at the initial time t_0.

The POD-ROM given by (20)-(21) usually works well for relatively smooth solutions where the largest R modes adequately capture the system dynamics. One of the main sources of inaccuracy in the POD-ROM is the truncation of the higher-order modes (from $R+1$ to ∞) in the reduced-order model. It has been shown that stabilization schemes improve the performance of the low-dimensional models [21], [22] and more recently more complex models have been proposed [5]–[8], [23]. The first and simplest model to overcome errors due to the finite truncation involved in the POD-ROM approach for stiff systems is called Heisenberg stabilization which uses a global constant eddy viscosity coefficient [6]. In large eddy simulations of turbulent flows this stabilization idea is also called mixing length closure, which is also used in POD literature [8]. This stabilization model accounts the effects of the truncated modes by using the same dissipation operators in the physical model by introducing a constant eddy viscosity coefficient in the model. Therefore, the corresponding physical parameter in the dissipation mechanism, which is Re number in our system, can be modified by adding an eddy viscosity coefficient in the following form

$$\frac{1}{Re}\Rightarrow\frac{1}{Re}(1+\nu_a), \tag{32}$$

where the free stabilization parameter ν_a is considered as a global constant for all the modes in this model (i.e., $\nu_e=\nu_a/Re$ is the total amount of eddy viscosity added to the system). The constant eddy viscosity idea suggested in (32) can be improved by supposing that the amount of dissipation is not identical for all the POD modes [24], [25]. Therefore, the global viscosity is replaced by modal viscosities using a linear kernel in the following form

$$\frac{1}{Re}\Rightarrow\frac{1}{Re}(1+\nu_a\frac{k}{R}), \tag{33}$$

where the constant ν_a is now defined as the amplitude of the eddy viscosity stabilization. Using a linear viscosity kernel, k/R, the amount of dissipation and hence stabilization increases linearly by the POD modal index k. Thus, we add more dissipation to the higher order modes, reflecting the locality of energy transfer between mode R and the discarded modes.

The problem is then to determine or to adjust the constant ν_a in these two eddy viscosity models to obtain better accuracy in the reduced-order model. An important feature of these eddy viscosity stabilization models is that they require minimal computational cost for computing reduced order model coefficients in (22)-(29). Therefore, a parameter study to find a suitable choice of the free parameter ν_a can be achieved with the minimal cost of solving (20)-(21). Specifying $\nu_a=0$ transforms these eddy viscosity ROM models to the standard POD-ROM model.

IV. NUMERICAL SCHEMES

The objective of the present work is to test and evaluate the characteristics of proper orthogonal decomposition reduced-order models (POD-ROM) and compare them with a solution

obtained by a direct numerical simulation (DNS) for solving incompressible Boussinesq equations. Here, we provide a brief description of the numerical methods employed in this study.

First of all, we implement compact difference schemes to approximate the differential operators (N, L, and D). A detailed stability and convergence analysis of the compact difference methods for flow problems [26] performed in [27] shows that it produces less numerical dissipation than standard schemes. As we mentioned above, the resulting ordinary differential equations are solved using a third order (TVD) Runge-Kutta scheme [28].

V. RESULTS

A. Differentially-Heated Cavity Problem

To illustrate the performance of POD-ROM given by (20)-(21), we first present results for a buoyancy driven flow enclosed in a differentially-heated tall cavity. A detailed description of the problem can be found at [29], [30]. The geometry of the problem is prescribed as a tall rectangular cavity in a $[0,1] \times [0,8]$ enclosure. The flow is driven by a constant temperature difference between the vertical walls. The temperature at the left wall ($x = 0$) is fixed at $\theta = 0.5$, and the right wall ($x = 1$) at $\theta = -0.5$. The top and bottom of the cavity ($y = 0$ and $y = 8$, respectively) are perfectly insulated (i.e., $\partial\theta/\partial y = 0$). No-slip boundary conditions are applied on all boundaries. The flow is initially at rest with a linear temperature distribution that matches the vertical walls. The Rayleigh number for this problem was chosen to be a supercritical value of $Ra = 3.4 \times 10^5$, the Richardson number is $Ri = 1$, and the Prandtl number $Pr = 0.71$. For the prescribed geometry, physical parameters, and boundary conditions, after an initial transient time, the flow exhibits a time-periodic behavior. The numerical simulations are performed until a final time $T = 1000$ which is sufficient enough for the flow settle into the periodic regime.

To build the POD-ROM, we first run a DNS computation on a fine mesh by using the resolution 128×1024 with a time step of $\Delta t = 0.004$. After a transient initial period, the flow exhibits a time-periodic behavior for the present configuration. We store 501 snapshots in time interval $[950, 1000]$ at equidistant time intervals. We then build our reduced-order model from this data set using the methodology discussed above. The decay of the POD eigenvalues are shown in Fig. 1. In Fig. 2, we provide contour plots for a few POD modes corresponding to the ω and θ fields to indicate the structure of the solutions. As we observe, the rapid decay in the eigenvalues corresponds to exceedingly smaller scale structures in the modes. This rapid decay indicates that solutions are likely smooth and can be accurately represented using relatively few ($R \approx 10$) modes for each scalar variable. Therefore, the eddy-viscosity modeling presented in (32) and (33) is not required for this problem.

In Table I, we provide estimates of the approximation quality of the POD bases for representing the given solution

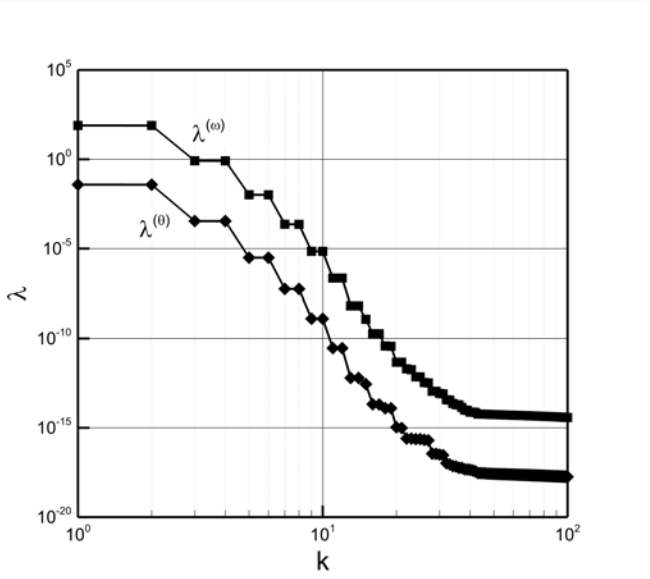

Fig. 1. Eigenvalues of the correlation matrix C for the differentially-heated cavity problem by using 500 snapshots.

TABLE I
POD ANALYSIS FOR DIFFERENTIALLY-HEATED CAVITY PROBLEM

R	P^ω	P^θ	CPU(s)	$\| e^\omega \|_2$	$\| e^\theta \|_2$
3	0.99468077	0.99540448	0.0459	3.0848E-1	6.5427E-3
6	0.99999701	0.99999852	0.1769	3.0442E-1	6.4753R-3
8	0.99999991	0.99999997	0.3889	3.0433E-1	6.4735R-3
10	1.0	1.0	0.7098	3.0433E-1	6.4735R-3

trajectories,

$$P^\omega(R) = \sum_{k=1}^{R} \lambda_k^\omega \Big/ \sum_{k=1}^{M} \lambda_k^\omega \quad \text{and} \quad P^\theta(R) = \sum_{k=1}^{R} \lambda_k^\theta \Big/ \sum_{k=1}^{M} \lambda_k^\theta,$$

as well as L^2 errors between the DNS and the POD-ROM at time $t = 1000$,

$$e^\omega = \omega^{\mathrm{ROM}} - \omega^{\mathrm{DNS}} \quad \text{and} \quad e^\theta = \theta^{\mathrm{ROM}} - \theta^{\mathrm{DNS}}$$

for varying numbers of basis functions. We also present the time required to solve the POD-ROM model (for comparison, the computational time for the DNS was $9531.14s$). We observe substantial reduction in computational time as well as accurate solutions for relatively small values of R.

B. Marsigli Flow Problem

In this section, we investigate the performance of the POD-ROM methodology by solving a strong shear flow exhibiting the Kelvin-Helmholtz instability, known as Marsigli flow or the lock-exchange problem. This flow problem is a convective flow problem and quite different than the periodic flow problem studied in previous section. Thus, the Marsigli flow is a more challenging benchmark problem for constructing accurate reduced-order models. The physical process in the Marsigli flow problem is motivated to explain how differences in density (i.e., by Boussinesq approximation, the density difference can be converted inversely proportional to

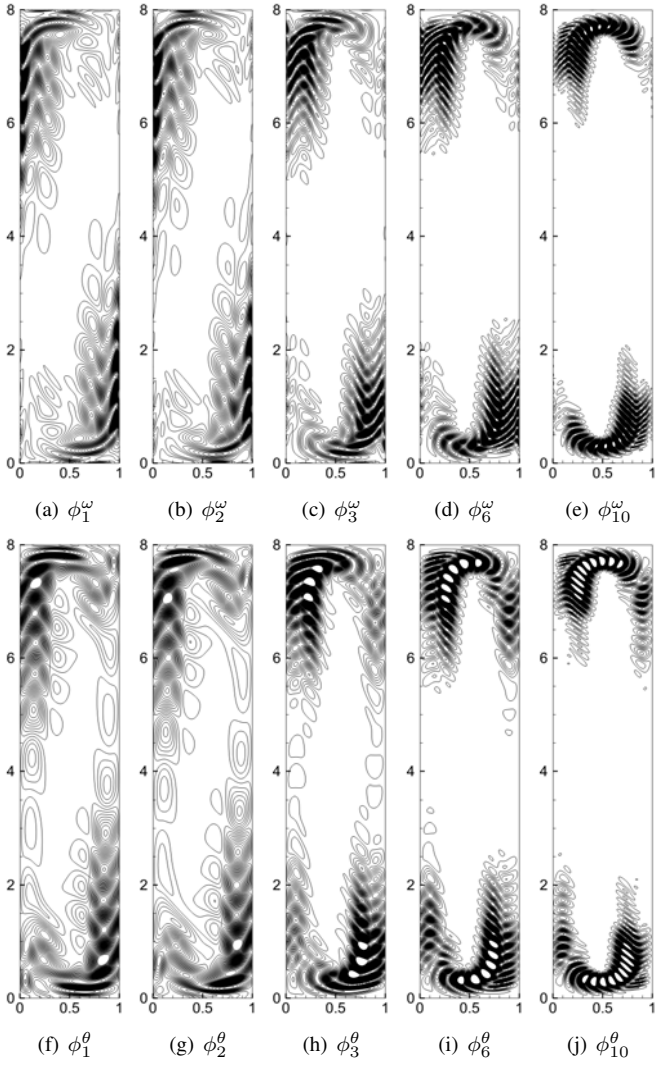

(a) ϕ_1^ω (b) ϕ_2^ω (c) ϕ_3^ω (d) ϕ_6^ω (e) ϕ_{10}^ω

(f) ϕ_1^θ (g) ϕ_2^θ (h) ϕ_3^θ (i) ϕ_6^θ (j) ϕ_{10}^θ

Fig. 2. Illustrative examples for some POD basis functions of the vorticity and temperature fields for the differentially-heated cavity problem.

temperature difference) cause currents to form in the ocean and seas. The setup used to perform numerical experiments is as follows as prescribed in [30]. Two fluids of different temperatures (corresponding to different densities) are initially at rest in a rectangular domain of $[0, 8] \times [0, 1]$ and separated by a vertical barrier at $x = 4$. The temperature is chosen to be $\theta = 1.5$ at the left half, which indicates lower density, and $\theta = 1$ at the right half, which indicate higher density. The flow is at rest initially (i.e., the vorticity and stream functions are set zero at $t = 0$) with constant temperature values for the left and right fluids given above. The no-slip and adiabatic boundary conditions are prescribed for the flow and temperature field, respectively. The lock-exchange flow is started by "removing the barrier." The values of the Reynolds, Richardson, and Prandtl numbers in simulations are selected as $Re = 5000$, $Ri = 4$, and $Pr = 1$. As highlighted in [30], the numerical simulation of this type of strong shear flow is quite challenging. We perform computations using a grid resolution of 4096×512

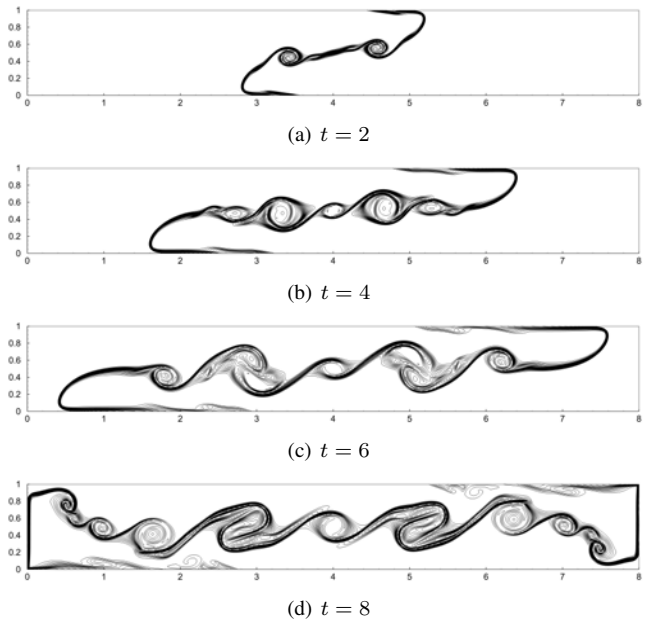

(a) $t = 2$

(b) $t = 4$

(c) $t = 6$

(d) $t = 8$

Fig. 3. Evolution of temperature field for the Marsigli flow problem at $Re = 5000$, $Ri = 4$, and $Pr = 1.0$ obtained by a DNS computation on a resolution of 4096×512.

with a time step of $\Delta t = 0.0005$.

The evolution of the temperature field is shown in Fig. 3 (with similar contours for the vorticity field, not shown). Once the flow is released at time $t = 0$, the flow is driven by the buoyancy force in Boussinesq system. An upper current flow, which moves from the left to the right side, and an undercurrent flow, which moves in the opposite direction, occur. Consequently, a strong shear layer is formed between upper and lower currents and this vortex sheets exhibits the Kelvin-Helmholtz instability. Progressively more vortical structures are generated, stretched and elongated as time goes on. The developments of the kinematic and thermal boundary layers are also shown in the plots. The numerical simulation of these convective rolling structures in flows exhibiting Kelvin-Helhmoltz instabilities is quite challenging and requires high-resolution to accurately capture the flow dynamics. Our DNS results are agree well with the results reported in Fig.1 and Fig.2 of [30]. One of the main objective in the our study is to test and evaluate the reduced-order models for this complex convective flow setting.

We store 401 snapshots between time interval $t \in [0, 8]$ in equidistant time intervals. These snapshots are used to create the POD basis for our reduced-order models. The corresponding eigenvalues are provided in Fig. 4.

The stiffness of this problem can be seen from this plot. Compared to the previous differentially-heated cavity flow problem, the eigenvalues for Marsigli flows slowly reduce their amplitude with increasing POD index. Therefore, it requires significantly more POD modes to capture the essential dynamics of the flow field. The analysis of the POD-ROM is summarized in Table II (for comparison, the DNS required 74.73 hours of computational time). The reduced-order model constructed using $R = 6$ modes captures 70% of

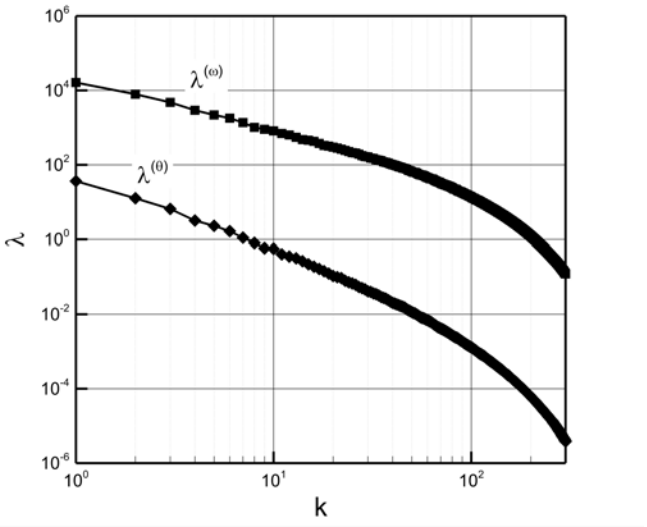

Fig. 4. Eigenvalues of the correlation matrix C for the Marsigli flow problem by using 400 snapshots at equidistant time intervals $t \in [0, 8]$.

TABLE II
POD ANALYSIS FOR THE MARSIGLI FLOW PROBLEM

R	P^{ω}	P^{θ}	CPU(s)	$\| e^{\omega} \|_2$	$\| e^{\theta} \|_2$
6	0.70537388	0.90322784	0.2299	3.7532	8.7977E-2
10	0.78600409	0.94733013	0.9208	2.9937	6.6690R-2
20	0.87584937	0.98036542	6.6110	2.3159	4.7504R-2
30	0.91786786	0.98997989	23.292	1.7466	2.8715R-2

energetics in this problem, whereas we report in Table I that the POD-ROM with $R = 6$ modes captures more than 99% in the previous problem. As expected, the accuracy of the reduced-order models increases with increasing R in POD-ROM models.

Fig. 5 shows the temperature isolines at time $t = 8$ comparing various reduced-order models with different R values with the DNS data. Similar comparisons can be seen with vorticity and stream function contours. This figure clearly demonstrates that an increase in R produces progressively more accurate reduced-order dynamical models since it includes more small scale effects associated with higher POD modes.

Next, we would like to address the effects of stabilization for this complex convective flow setting. A parametric study performed by systematically varying ν_a is performed. Fig. 6 shows the influence of the ν_a parameter on the accuracy of the temperature field when including the Heisenberg constant eddy viscosity stabilization given by (32). We compute L^2 norms of temperature field at time $t = 8$ for reduced-order models with $R = 6$ and $R = 10$. As we can see from the figure, stabilization slightly improves the accuracy of the models. Optimal values for the stabilization parameters become $\nu_a = 0.55$ for $R = 6$ and $\nu_a = 0.25$ for $R = 10$. Similar observations can be seen from the Rempfer's mode dependent eddy viscosity stabilization scheme given by (33).

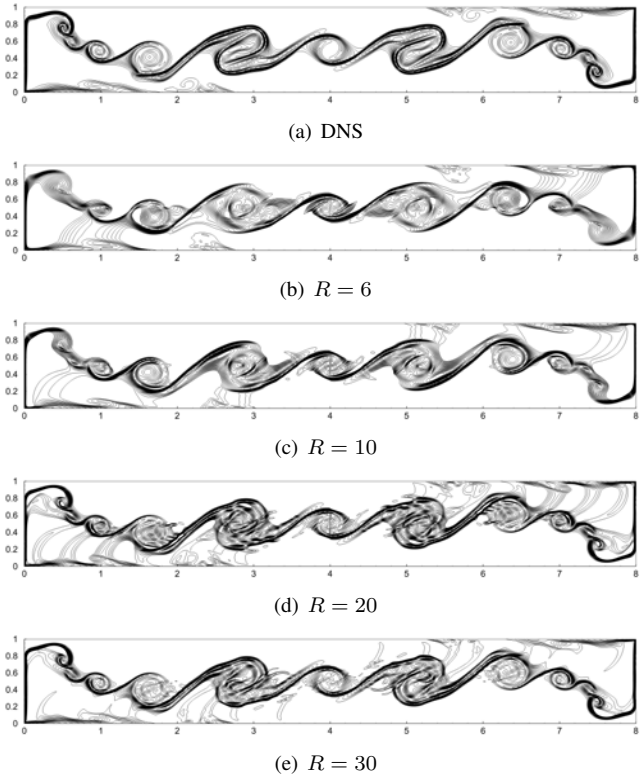

(a) DNS

(b) $R = 6$

(c) $R = 10$

(d) $R = 20$

(e) $R = 30$

Fig. 5. Temperature contour plots for the Marsigli flow problem at time $t = 8$ showing a comparison of POD-ROMs with various R with the DNS data.

With this stabilization model, optimal values are $\nu_a = 1.1$ for $R = 6$ and $\nu_a = 1.6$ for $R = 10$. Because of the definition of linear viscosity kernel as k/R in the Rempfer's model, the optimal value for the $R = 10$ case is greater than that of the $R = 6$. It can be noted that $\nu_a = 0$ here corresponds to the standard POD-ROM Galerkin model. Using these optimal values, we next compare the results for $R = 10$ in Fig. 8, plotting the temperature fields at time $t = 8$. It is clear that we obtain slightly more accurate results using the eddy viscosity stabilization. Although there is not much difference between the Heissenberg's and Rempfer's stabilization models when we use their optimal values, it can be seen that Rempfer's model predicts slightly better results. However, it is possible to obtain more accurate results with eddy viscosity stabilization, we can also see that an increase of R is more effective in terms of accuracy. For example, standard POD-ROM model using $R = 10$ modes without performing any stabilization (i.e., Galerkin model) yield more accurate results than the stabilized model with $R = 6$ modes.

The analysis presented above uses the same eddy viscosity correction for the vorticity and temperature transport equations in the model. Therefore, the same amount of ν_a is used in (20)-(21) for stabilized POD-ROM models. In the following, we also perform a stability analysis with respect to the ν_a in such a way that we independently applied different values of ν_a for vorticity and temperature transport equations. Fig. 9 shows the sensitivity plot for reduced-order

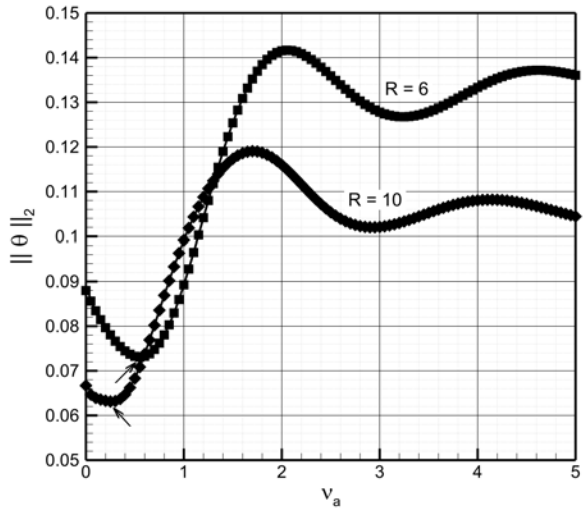

Fig. 6. Sensitivity analysis with respect to the free stabilization parameter ν_a for reduced-order models with $R = 6$ and $R = 10$ using the Heisenberg's constant eddy viscosity stabilization given by Eq. (32). The L^2 norms of temperature field are computed at time $t = 8$. Optimal values for the stabilization parameters become $\nu_a = 0.55$ for $R = 6$ and $\nu_a = 0.25$ for $R = 10$.

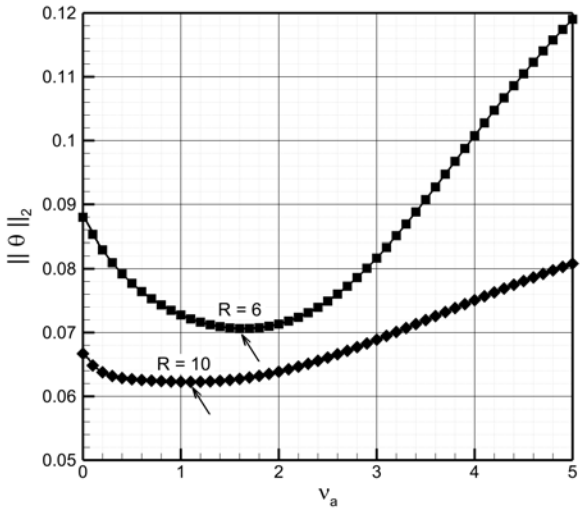

Fig. 7. Sensitivity analysis with respect to the free stabilization parameter ν_a for reduced-order models with $R = 6$ and $R = 10$ using the Rempfer's mode dependent eddy viscosity stabilization given by Eq. (33). The L^2 norms of temperature field are computed at time $t = 8$. Optimal values for the stabilization parameters become $\nu_a = 1.1$ for $R = 6$ and $\nu_a = 1.6$ for $R = 10$.

models with $R = 6$ using the Rempfer's mode dependent eddy viscosity stabilization given by Eq. (33). The values of free stabilization parameter ν_a are varied independently for (20)-(21). Optimal values for the ν_a are as follows: $\nu_a = 1.2$ for vorticity transport equation modeled in Eq. (20) and $\nu_a = 4.4$ for temperature transport equation given by Eq. (21). The computed L_2 norm for the temperature $\| \theta \| = 0.0689$ whereas the $\| \theta \| = 0.0879$ for the Galerkin method in which $\nu_a = 0$ for both vorticity and temperature equations. This analysis also demonstrates that the optimal amount of eddy viscosity stabilization is not the same for momentum and energy equations. If we apply eddy viscosity stabilization to only momentum equations (i.e., vorticity transport equation) the L^2 norm becomes approximately $\| \theta \| = 0.0736$. We also emphasize that the L^2 norm of temperature field for POD-ROM with $R = 10$ is $\| \theta \| = 0.0666$. As we can see that, however, we obtain slightly more accurate results by using stabilization schemes for optimal values of eddy viscosity parameter, with a negligible small computational overload, the performance of the POD-ROM depends more on the number of modes than the amount of eddy viscosity stabilization for this type of convective flow problems.

VI. CONCLUSIONS

We provide two benchmark studies for constructing POD-ROM for the two-dimensional incompressible Boussinesq equations: the differentially-heated cavity and Marsigli flow. In our first example, we demonstrate that the dynamics of the quasi-periodic flow is well captured by the proposed POD-ROM even using just a few modes. In our second example, however, we showed that the POD-ROM requires more modes and can benefit from the addition of eddy viscosity stabilization. We compared Heisenberg's constant and Rempfer's mode dependent eddy viscosity models to the standard Galerkin projection without stabilization. Parameter studies were performed to identify the ideal values of the eddy viscosity parameters and show improvement in using different values of eddy viscosity in the vorticity and energy equations. These studies were based on the standard POD method for building a basis for a given simulation. In a follow up study, we plan to use the Marsigli flow problem to study the impact of accurately choosing the time intervals over which POD bases are calculated [31] on both the accuracy of the POD-ROM as well as the optimal values of the stabilization parameters as well as investigate the accuracy of these models as the parameter Ri varies by extending the methods in [32].

REFERENCES

[1] K. Ito and S. Ravindran, "A reduced-order method for simulation and control of fluid flows," *Journal of Computational Physics*, vol. 143, no. 2, pp. 403–425, 1998.

[2] A. Iollo, S. Lanteri, and J.-A. Désidéri, "Stability properties of POD–Galerkin approximations for the compressible Navier–Stokes equations," *Theoretical and Computational Fluid Dynamics*, vol. 13, no. 6, pp. 377–396, 2000.

[3] A. Hay, J. T. Borggaard, and D. Pelletier, "Local improvements to reduced-order models using sensitivity analysis of the proper orthogonal decomposition," *Journal of Fluid Mechanics*, vol. 629, no. 1, pp. 41–72, 2009.

[4] E. Arian, M. Fahl, and E. W. Sachs, "Trust-region proper orthogonal decomposition for optimal flow control," ICASE, Tech. Rep. ICASE-2000-25, 2000.

[5] V. L. Kalb and A. E. Deane, "An intrinsic stabilization scheme for proper orthogonal decomposition based low-dimensional models," *Physics of fluids*, vol. 19, p. 054106, 2007.

[6] M. Bergmann, C.-H. Bruneau, and A. Iollo, "Enablers for robust POD models," *Journal of Computational Physics*, vol. 228, no. 2, pp. 516–538, 2009.

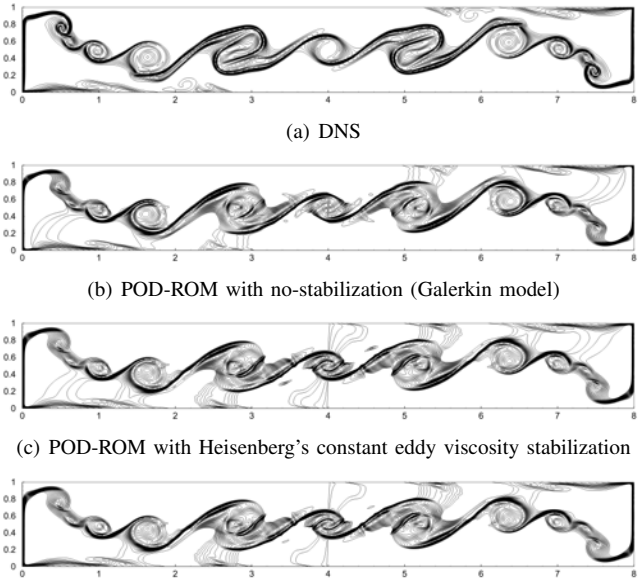

(a) DNS

(b) POD-ROM with no-stabilization (Galerkin model)

(c) POD-ROM with Heisenberg's constant eddy viscosity stabilization

(d) POD-ROM with Rempfer's mode dependent eddy viscosity stabilization

Fig. 8. Temperature contour plots for the Marsigli flow problem at time $t = 8$ using $R = 10$ modes by comparing the stabilization schemes.

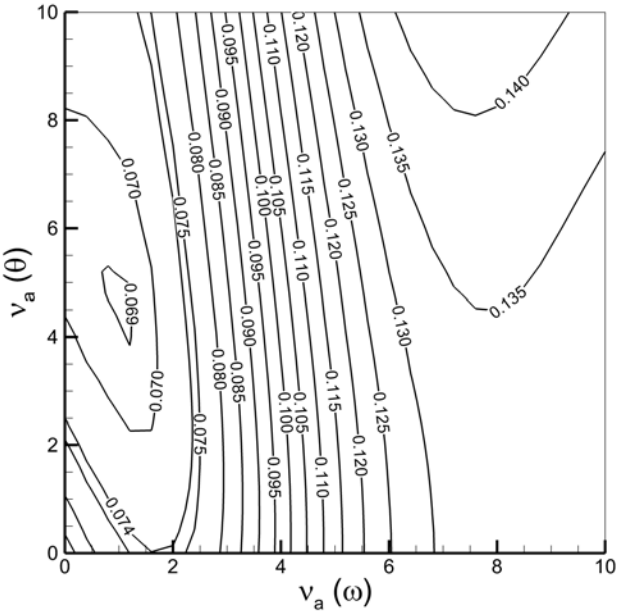

Fig. 9. Parametric study of ν_a for a POD-ROM with $R = 6$ using Rempfer's mode dependent eddy viscosity (33).

[7] J. Borggaard, T. Iliescu, and Z. Wang, "Artificial viscosity proper orthogonal decomposition," *Mathematical and Computer Modelling*, vol. 53, no. 1, pp. 269–279, 2011.

[8] Z. Wang, I. Akhtar, J. Borggaard, and T. Iliescu, "Proper orthogonal decomposition closure models for turbulent flows: a numerical comparison," *Computer Methods in Applied Mechanics and Engineering*, vol. 237–240, pp. 10–26, 2012.

[9] M. Couplet, P. Sagaut, and C. Basdevant, "Intermodal energy transfers in a proper orthogonal decomposition-Galerkin representation of a turbulent separated flow," *Journal of Fluid Mechanics*, vol. 491, pp. 275–284, 2003.

[10] B. R. Noack, K. Afanasiev, M. Morzyński, G. Tadmor, and F. Thiele, "A hierarchy of low-dimensional models for the transient and post-transient cylinder wake," *Journal of Fluid Mechanics*, vol. 497, pp. 335–363, 2003.

[11] A. E. Deane and L. Sirovich, "A computational study of Rayleigh-Bénard convection. Part 1. Rayleigh-number scaling," *Journal of Fluid Mechanics*, vol. 222, pp. 231–250, 1991.

[12] L. Sirovich and A. E. Deane, "A computational study of Rayleigh–Bénard convection. Part 2. Dimension considerations," *Journal of Fluid Mechanics*, vol. 222, no. 1, pp. 251–265, 1991.

[13] H. Gunes, A. Liakopoulos, and R. Sahan, "Low-dimensional description of oscillatory thermal convection: the small Prandtl number limit," *Theoretical and Computational Fluid Dynamics*, vol. 9, no. 1, pp. 1–16, 1997.

[14] A. Liakopoulos, P. Blythe, and H. Gunes, "A reduced dynamical model of convective flows in tall laterally heated cavities," *Proceedings of the Royal Society of London. Series A: Mathematical, Physical and Engineering Sciences*, vol. 453, no. 1958, pp. 663–672, 1997.

[15] R. Sahan, A. Liakopoulos, and H. Gunes, "Reduced dynamical models of nonisothermal transitional grooved-channel flow," *Physics of Fluids*, vol. 9, p. 551, 1997.

[16] B. Podvin and P. Le Quéré, "Low-order models for the flow in a differentially heated cavity," *Physics of Fluids*, vol. 13, p. 3204, 2001.

[17] N. Hasan and S. Sanghi, "Proper orthogonal decomposition and low-dimensional modelling of thermally driven two-dimensional flow in a horizontal rotating cylinder," *Journal of Fluid Mechanics*, vol. 573, pp. 265–296, 2007.

[18] L. Sirovich, "Turbulence and the dynamics of coherent structures. I-Coherent structures. II-Symmetries and transformations. III-Dynamics and scaling," *Quarterly of Applied Mathematics*, vol. 45, pp. 561–571, 1987.

[19] P. Holmes, J. L. Lumley, and G. Berkooz, *Turbulence, coherent structures, dynamical systems and symmetry*. Cambridge University Press, 1998.

[20] S. Ravindran, "A reduced-order approach for optimal control of fluids using proper orthogonal decomposition," *International Journal for Numerical Methods in Fluids*, vol. 34, no. 5, pp. 425–448, 2000.

[21] N. Aubry, P. Holmes, J. L. Lumley, and E. Stone, "The dynamics of coherent structures in the wall region of a turbulent boundary layer," *Journal of Fluid Mechanics*, vol. 192, pp. 115–173, 1988.

[22] L. Sirovich and X. Zhou, "Reply to "observations regarding 'coherence and chaos in a model of turbulent boundary layer' by x. zhou and l. sirovich [phys. fluids a 4, 2855 (1992)]"," *Physics of Fluids*, vol. 6, no. 4, pp. 1579–1582, 1994.

[23] J. Borggaard, A. Duggleby, A. Hay, T. Iliescu, and Z. Wang, "Reduced-order modeling of turbulent flows," in *Proceedings of the 18th International Symposium on Mathematical Theory of Networks & Systems*, 2008.

[24] D. Rempfer, "Kohärente Strukturen und Chaos beim laminar-turbulenten Grenzschichtumschlag," Ph.D. dissertation, University of Stuttgart, 1991.

[25] W. Cazemier, "Proper orthogonal decomposition and low dimensional models for turbulent flows," Ph.D. dissertation, Rijksuniversiteit Groningen, 1997.

[26] S. K. Lele, "Compact finite difference schemes with spectral-like resolution," *Journal of Computational Physics*, vol. 103, no. 1, pp. 16–42, 1992.

[27] C. Wang and J.-G. Liu, "Analysis of finite difference schemes for unsteady Navier-Stokes equations in vorticity formulation," *Numerische Mathematik*, vol. 91, no. 3, pp. 543–576, 2002.

[28] S. Gottlieb and C.-W. Shu, "Total variation diminishing Runge-Kutta schemes," *Mathematics of Computation*, vol. 67, no. 221, pp. 73–85, 1998.

[29] H. Johnston and R. Krasny, "Fourth-order finite difference simulation of a differentially heated cavity," *International Journal for Numerical Methods in Fluids*, vol. 40, no. 8, pp. 1031–1037, 2002.

[30] J.-G. Liu, C. Wang, and H. Johnston, "A fourth order scheme for incompressible Boussinesq equations," *Journal of Scientific Computing*, vol. 18, no. 2, pp. 253–285, 2003.

[31] J. Borggaard, A. Hay, and D. Pelletier, "Interval-based reduced-order models for unsteady fluid flow," *International Journal of Numerical Analysis and Modeling*, vol. 4, no. 3–4, pp. 353–367, 2007.

[32] A. Hay, J. Borggaard, and D. Pelletier, "Local improvements to reduced-order models using sensitivity analysis of the proper orthogonal decomposition," *Journal of Fluid Mechanics*, vol. 629, pp. 41–72, 2009.